pp 1192–1208.
doi:10.1017/aer.2021.15

Numerical study of geometric morphing wings of the 1303 UCAV

B. Nugroho
bagus.nugroho@unimelb.edu.au
Mechanical Engineering
The University of Melbourne
Melbourne
Australia

J. Brett
Synergetics Consulting Engineers
Melbourne
Australia

B.T. Bleckly and R.C. Chin
Mechanical Engineering
The University of Adelaide
Adelaide
Australia

ABSTRACT

Unmanned Combat Aerial Vehicles (UCAVs) are believed by many to be the future of aerial strike/reconnaissance capability. This belief led to the design of the UCAV 1303 by Boeing Phantom Works and the US Airforce Lab in the late 1990s. Because UCAV 1303 is expected to take on a wide range of mission roles that are risky for human pilots, it needs to be highly adaptable. Geometric morphing can provide such adaptability and allow the UCAV 1303 to optimise its physical feature mid-flight to increase the lift-to-drag ratio, manoeuvrability, cruise distance, flight control, etc. This capability is extremely beneficial since it will enable the UCAV to reconcile conflicting mission requirements (e.g. loiter and dash within the same mission). In this study, we conduct several modifications to the wing geometry of UCAV 1303 via Computational Fluid Dynamics (CFD) to analyse its aerodynamic characteristics produced by a range of different wing geometric morphs. Here we look into two specific geometric morphing wings: linear twists on one of the wings and linear twists at both wings (wash-in and washout). A baseline CFD of the UCAV 1303 without any wing morphing is

Received 16 September 2020; revised 25 December 2020; accepted 18 February 2021.

validated against published wind tunnel data, before proceeding to simulate morphing wing configurations. The results show that geometric morphing wing influences the UCAV-1303 aerodynamic characteristics significantly, improving the coefficient of lift and drag, pitching moment and rolling moment.

Keywords: UCAV; CFD; Morphing Wings

NOMENCLATURE

Re	Reynolds number
Re_c	mean aerodynamic chord Reynolds number
M	Mach number
C_P	pressure coefficient
C_L	lift coefficient
C_D	drag coefficient
C_{MP}	pitching moment coefficient
C_{MR}	roll moment coefficient

Greek Symbol

α	angle-of-attack
η	semi-span reference

1.0 INTRODUCTION

Unmanned Combat Aerial Vehicles (UCAVs) are believed by many to be the future of aerial strike/reconnaissance system because of their advantages over traditional crewed combat aircraft, such as a much lower risk to operator's life, a smaller size and a reduced cost[1,2]. In the last two decades, much attention has been paid to a particular future UCAV concept, the UCAV 1303. The UCAV 1303 was originally designed by the Boeing Phantom Works and the US Airforce Lab (AFRL) in the late 1990s and scheduled to operate in the 2020 time frame[1,3,4]. Later, the design fell under The Technical Cooperation Program (TTCP), a joint defence-related forum between the United States, United Kingdom, Australia, New Zealand and Canada. The aircraft is a tail-less Blended Wing Body (BWB) (see Ordoukhanian and Madni[5] for further details about BWB design) with a lambda wing configuration (Fig. 1). It has 47° leading edge sweep angle and ±30° trailing edge sweep. The lambda wing design can be identified from the existence of a convex trailing edge crank (wing sweep changes) near both of the wing tips and a concave trailing edge crank at the mid-semi-span[3]. The vehicle is designed to be powered by a single un-reheated turbofan engine located on the centreline with expandable fuel tank, and it has two internal payload bays at either side of the engine[1,2].

Initial studies and developments of the UCAV 1303 aerodynamics performance for the TTCP in the early 2000s involved many aspects, such as wind tunnel experiments[3,7], numerical Computational Fluid Dynamics (CFD)[8,9] and Conceptual Design and Optimisation (CDO)[1,2]. These studies reveal that the UCAV 1303 is sensitive to Reynolds number. As Re_c increases, the UCAV 1303 lift coefficient C_L, drag coefficient C_D and pitching moment

https://doi.org/10.1017/aer.2021.15 Published online by Cambridge University Press

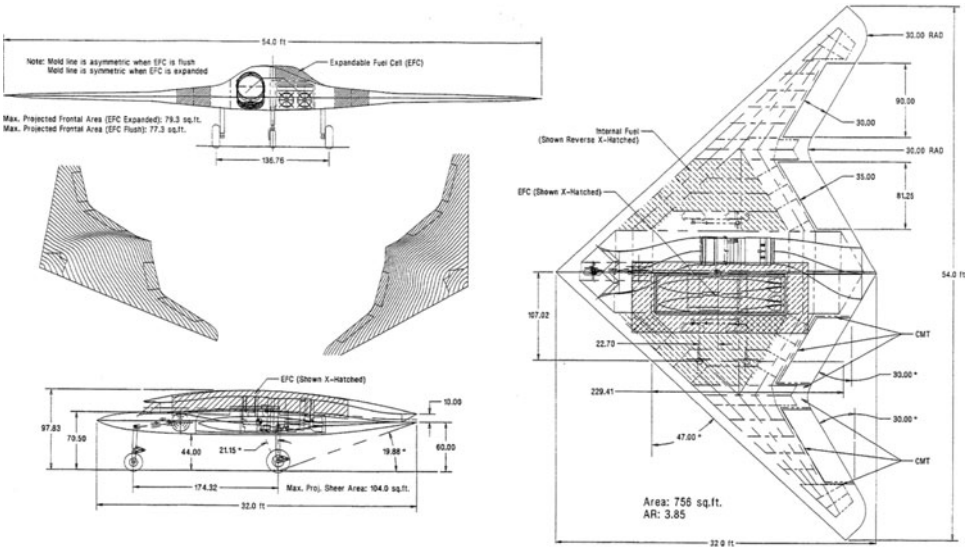

Figure 1. UCAV-1303 design plan by the Boeing Phantom Works and AFRL[6].

coefficient C_{MP} vary significantly with the angle-of-attack α. Furthermore, the TTCP studies also show that the UCAV 1303 tends to be unstable even at low angles of attack.

Unlike standard aircraft, the UCAV 1303 design does not incorporate a vertical tail and has minimum control surfaces. Furthermore, it has a stealthy design which makes it operate at close to the limit of flight stability[10,11]. The UCAV 1303 design has been subjected to many aerodynamic control studies, both computational and experimental, such as using traditional surface control (flaps and ailerons)[12,13], active flow control with synthetic jets[14] and even plasma actuators[15–18]. One flight control method for the UCAV 1303 that has not been discussed in great detail is the morphing wing technology. The idea of the morphing wing is inspired by nature, particularly birds and flying mammals (i.e. bats). Utilising their muscle, skeleton and feathers, birds can sweep their wings at high speed and spread their wings in turns or decelerate[19]. The term morphing is defined as a set of technologies that increase a vehicle's performance by manipulating certain characteristics to better match the vehicle state to the environment and task at hand[20,21]. Such systems provide superior system capabilities, which will enable the aircraft to undertake a wide range of missions with changing parameters. The simplest parts of an aircraft to change during a flight are the wings. They can undergo changes in geometry (e.g. span, area, chord, sweep, etc.) such that the wing configuration is optimised for widely varying flight conditions (e.g. loiter, dash and high-speed manoeuvres)[22]. This morphing wing ability has the potential to revolutionise future military and commercial aircraft.

In this report, we will conduct an investigation into several possible morphing wing methods that would result in improved manoeuvring performances and stabilities of the UCAV 1303. The investigation is conducted via CFD simulation using a commercial-based software FLUENT-ANSYS. To validate the CFD solver, we conduct a baseline model CFD simulation and compare the results with published wind tunnel data for the UCAV 1303. Following this, we investigate several morphing cases, such as a linear twist on a section of one of the outer wings of the UCAV-1303 (which allows the model to perform rolling movement), and twists at both wings which force the flow to remain attached at a high angle-of-attack α (wash-in and

https://doi.org/10.1017/aer.2021.15 Published online by Cambridge University Press

washout). The linear twist on one of the wings is compared with a more traditional surface control such as elevons.

2.0 NUMERICAL METHOD

In this study, we use FLUENT software package by Ansys, with incompressible Reynolds Averaged Navier–Stokes (RANS) solver and turbulence model $k-\omega$ SST (Shear Stress Transport). We chose this turbulent model based on the report by Wong et al.[23] and Arthur and Petterson[24] where it was found that $k-\omega$ SST turbulent model can resolve the near-wall flow relatively well (see Monk and Chadwick[25] for comparison of various turbulence model simulations on UCAV-1303). We also choose incompressible flow because the simulation is run at a low Mach number (0.25 Mach). The freestream turbulence intensity value is set at 5% with turbulent viscosity ratio of 0.01. Note that these values were chosen arbitrarily because of the lack of information in the corresponding experimental data. We have tested several different turbulence intensity values; however, we found no significant differences in the final results.

The meshing in this study is constructed using ANSYS ICEM CFD package via unstructured tetrahedral mesh, generated by the Delaunay triangulation method, to best capture the UCAV 1303 complex geometry and resolve the sharp edge at the wing tip[26,27]. The mesh is set to have five prism layers over the fuselage and wings of the UCAV-1303 model. Here we set the prism growth rate as 1.3, and the layer thickness was selected to cover $30 < y^+ < 300$ (where $y^+ = U_\tau y/\nu$, y is the wall normal distance, U_τ is skin friction velocity and ν is kinematic velocity). Note that the majority of the cells are in the range of $30 < y^+ < 100$, where most of the turbulence energy resides[28,29]. To ensure that our mesh is proper, several different mesh qualities were investigated (including different mesh settings and numbers). The mesh arrangements which produced results that are mostly independent of different mesh settings, whilst keeping the total mesh number minimal, are selected as the final mesh.

The UCAV 1303 model mesh is placed in the centre of a full sphere with a radius of ≈ 10 root chords. This length provides sufficient distance to prevent any boundary interactions. Furthermore, the spherical shape allows for a single mesh to be used over multiple angles of attack α, via changes in the boundary condition. Various initial studies by the TTCP show that the UCAV 1303 is sensitive to sharp edges, i.e. in the leading edge and wing tip[3,7]. To overcome this issue, we generated a finer mesh at these locations. In this study, we use either half or the entire UCAV 1303 model. The half model is used when there are no differences between the port side and the starboard side of the UCAV 1303, i.e. baseline case or when both wings are morphed. This half model would allow us to use less computational resources. However, for a case where one of the wings is modified, we use the full model. This attention to detail resulted in a mesh with approximately 1.7 million cells for the half-model baseline body simulation and 3.4 million cells for the full model simulation. In this study, we use Fig. 2 as the wing semi-span reference locations.

3.0 MODEL VALIDATION AND BASE CASE

To ensure that our simulation is valid, we conduct a baseline simulation model to match the experimental data from Bruce and Mundell[30] and McParlin et al.[3]. Here, the baseline simulation is conducted at a Mach number of 0.25 with Reynolds number of 5.6×10^6 based on the mean aerodynamic chord (the simulated model has a similar dimension as the experiment model). The simulation was conducted at angles of attack $\alpha =$

https://doi.org/10.1017/aer.2021.15 Published online by Cambridge University Press

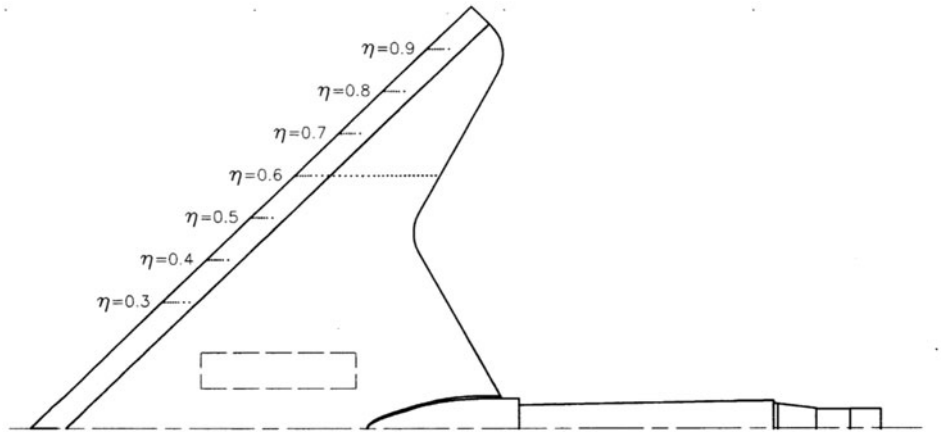

Figure 2. Semi-span details (taken from Ref. (3)).

0°, 5°, 7°, 8°, 9°, 10°, 12.5°, 15°. We did not go beyond $\alpha > 15°$, because we assume such an angle would exceed the onset of the unstable condition, and it is outside the scope of this study. Figure 3 shows a comparison between the experiment data (black solid square)[3,30] and the CFD (black open circle) results from the current study, where (a) is coefficient of lift versus angle-of-attack, (b) coefficient of drag versus angle-of-attack, (c) pitching moment coefficient versus angle-of-attack and (d) ratio of coefficient of lift and drag versus angle-of-attack.

The coefficient of lift from the CFD results agrees well with the experimental data, while the coefficient of drag from the numerical simulations show slightly higher values than that of the experiments (although the curve is similar). The wind tunnel experiment that was conducted by Bruce and Mundell[30] and McParlin et al.[3] involves a large sting cylinder attached to the rear of the UCAV 1303 model for support. We believe that this discrepancy is due to the absence of the sting support (which would affect the flow field) on the rear of our simulation. The slightly higher C_D numerical simulation translates to a lower ratio of coefficient of lift and drag at $0° < \alpha < 12.5°$ (Fig. 3(d)). The pitching moment coefficient from the CFD shows good agreement with the experiment data at $\alpha < 10°$. Beyond this angle-of-attack, the C_{MP} deviates slightly compared with the experimental data. Although the C_{MP} from our CFD slightly deviates, it exhibits a higher accuracy compared to that of the TTCP CFD simulations (see Wong et al.[23] for the TTCP CFD results). The UCAV 1303 tends to experience pitch break at $\alpha \approx 8° - 9°$. This behaviour has been well documented for UCAV 1303, and it is caused by the large-scale leading-edge vortices that grow and move further from the fuselage centreline towards the outer edge of the wings.

Figure 4 shows the flow visualisation of the streamlines from above the leading edge. At a low angle-of-attack ($\alpha \leq 5°$), there is no flow separation. At $\alpha = 7°$, the flows on the trailing edge of section $\eta = 0.6 - 0.8$ (Fig. 2) tend to move towards the outer edge of the wing. At higher angle-of-attacks ($\alpha = 8°$ and 9°), large-scale helical structures formed at $\eta \approx 0.5$, and these vortices also move towards the outer edge of the wing (trailing edge of $\eta \approx 0.8$ to 1.0). As the α is increased further towards 12.5° and 15°, the source of the vortical motion moves further towards the nose tip of the UCAV 1303 and becomes larger in size. Interestingly, these large vortical structures that leave the trailing edge move closer to the centre line of the UCAV-1303 (trailing edge of $\eta \approx 0.5$ to 0.6). These large vortical structures and unique flows are also recorded on the oil film experiment by McParlin et al.[3], and they are believed to be

https://doi.org/10.1017/aer.2021.15 Published online by Cambridge University Press

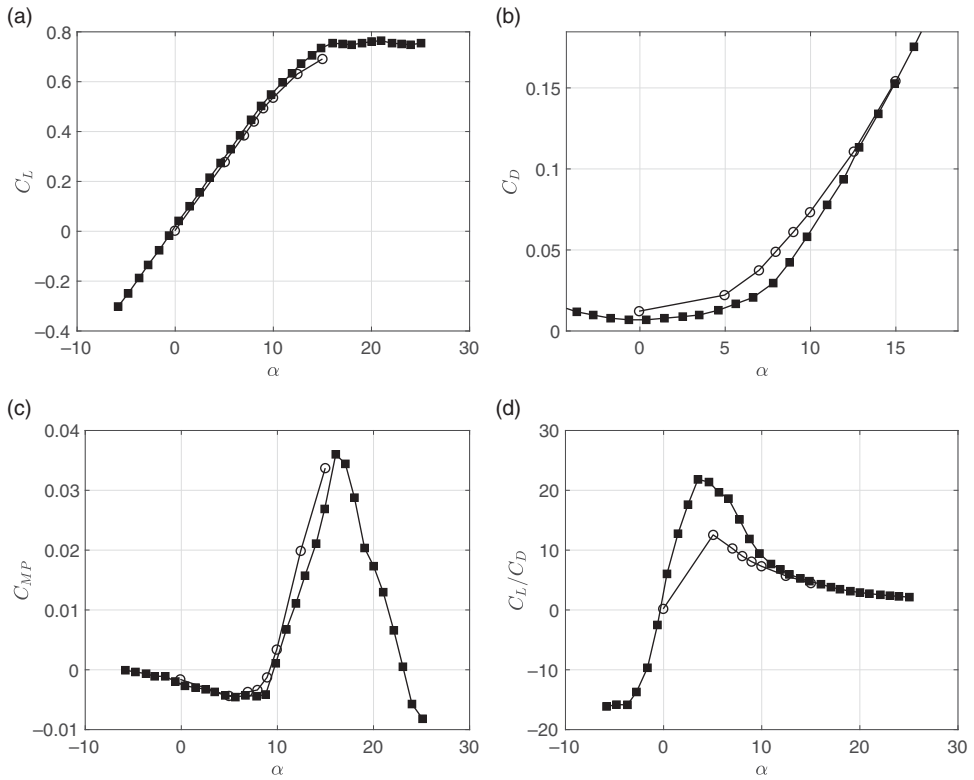

Figure 3. Matching experiment (closed black square) and CFD (open black circles) data with (a) C_L, (b) C_D, (c) C_{MP} and (d) C_L/C_D. Experiment data are taken from Refs. (3,30): $Re_c = 5.6 \times 10^6$ (black ■). CFD data from current study at $Re_c = 5.6 \times 10^6$ (black open ○).

the cause of instability of the UCAV 1303 at a high angle-of-attack, i.e. at $\alpha > 10°$. The CFD of the baseline UCAV 1303 model in this study closely matched the experimental data. Hence, it provides confidence to extend the study further and to conduct wing profile modifications as discussed in the following sections.

4.0 GEOMETRIC MODIFICATIONS

For this study, we will investigate the geometric modifications in the form of elevons as a traditional surface control, as well as two cases of morphing wings, i.e. linear twists on one of the wings and linear twists at both wings (wash-in and washout). Here, the meshing and the computational solver settings are set to mimic the baseline studies in the previous section. One main difference is that, for the elevons and linear twist cases, the simulation will be conducted on full models, doubling the total mesh size. In the case of linear twist at both wings (wash-in and washout), the simulation is conducted at half body, because of the symmetry and to save computational power. The geometric modifications are conducted via a modification of the geometry portion of the save file from ICEM-CFD using a custom MATLAB script. The modified geometry and morphing are then checked for errors using ICEM-CFD, and finally, a three-dimensional (3D) mesh can be produced over the new geometry file. Note that

https://doi.org/10.1017/aer.2021.15 Published online by Cambridge University Press

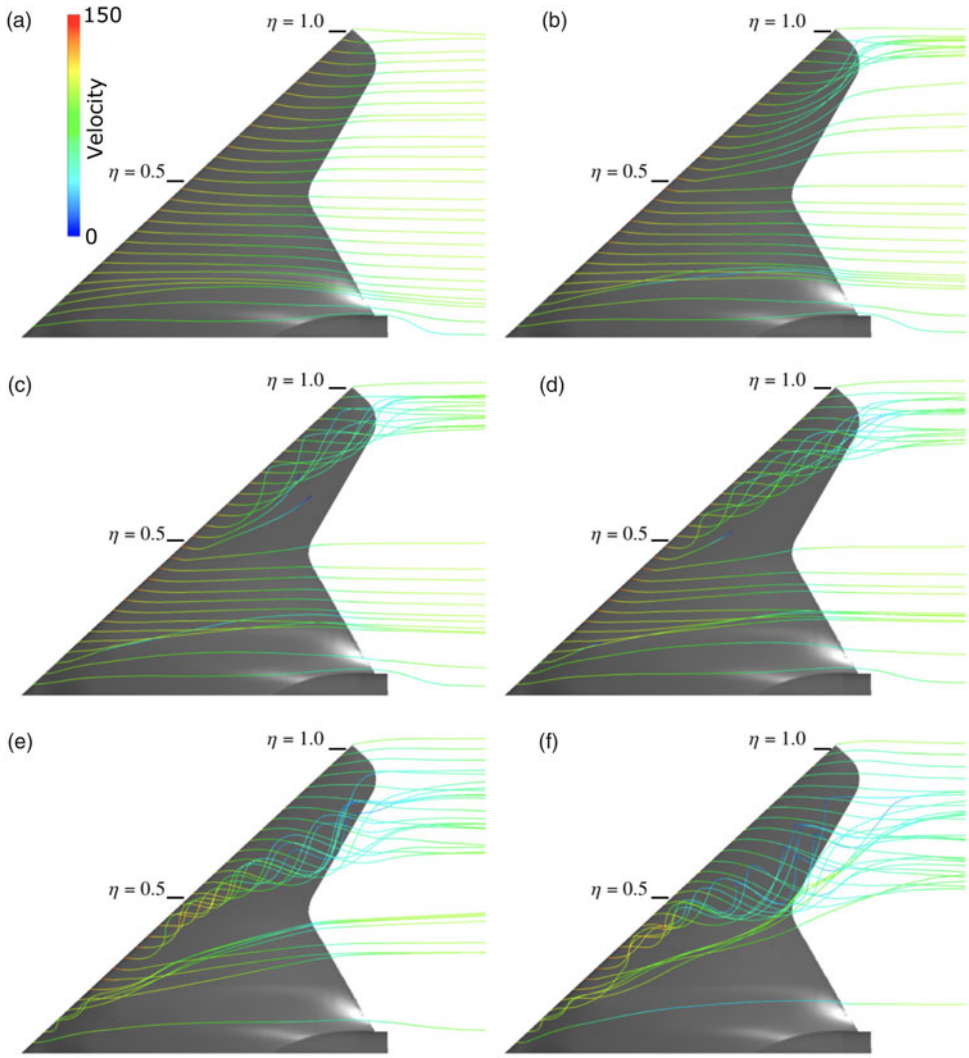

Figure 4. Set of 30 streamlines released from a rake a short distance above the leading edge of wing, coloured by velocity, for selected angles of attack: (a) $\alpha = 5°$, (b) $\alpha = 7°$, (c) $\alpha = 8°$, (d) $\alpha = 9°$, (e) $\alpha = 12.5°$, (f) $\alpha = 15°$

we acknowledge that there are many other possible geometry modifications, such as using rounded leading edge to improve the coefficient of moment. However, in this report we having chosen to focus on the wing twisting because we are also interested to investigate how well it can generate a rolling moment.

4.1 Elevons as surface control

In this section, we will examine the aerodynamic effects of traditional elevons as a surface flow control. This analysis would allow us to compare the roll moments from the morphing wing cases, which will be presented in later sections. Figure 5 shows the locations of the

https://doi.org/10.1017/aer.2021.15 Published online by Cambridge University Press

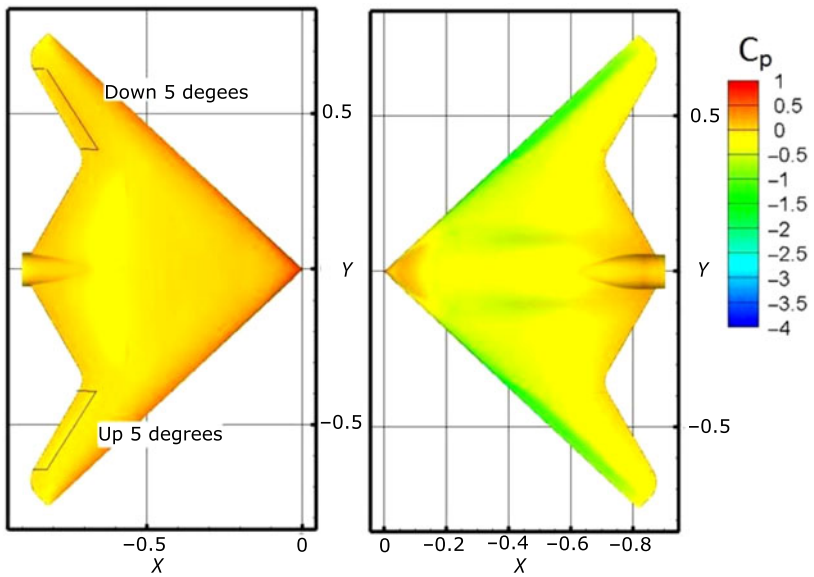

Figure 5. UCAV 1303 with the elevons location, coefficient of pressure C_P contours at an angle-of-attack of 7°. The left-hand images show underside, and the right-hand side shows top surface of the UCAV 1303.

elevons, and it is overlaid with the coefficient of pressure C_P contours at an angle-of-attack of 7°. The elevons are located at the outer wing section of the UCAV 1303 to generate maximum roll moments. The elevons are modelled by twisting the wing in an upward or downward direction at 5°. Note that this angle was chosen arbitrarily, and it was considered sufficient for a velocity of Mach 0.25 (the flight envelope of the simulation and wind tunnel testing). The CFD simulations were conducted at angle-of-attacks $\alpha = 5°$, 7°, 8° and 9°. These angles are chosen as the appropriate representation where the UCAV 1303 is likely to operate before the onset of pitch break/instability (Fig. 3(c)).

Figure 6 shows the aerodynamic properties of UCAV 1303 with elevons, i.e. (a) coefficients of lift, (b) coefficient of drag, (c) coefficient of pitching moment, (d) coefficient of rolling moment and (e) ratio between coefficient of lift and drag. The coefficient of lift and drag plots show that there are not many differences between the baseline case and the elevon case (apart from the C_D at 5°). The almost identical coefficients of lift C_L and coefficients of drag C_D values are probably due to the location of the elevons (which is on the trailing edge, and contributes little to the lift generated), and their directions are anti-symmetrical (one is upward and the other is downward). The ratio of C_L to C_D (Fig. 6(e)) shows that, in general, the baseline UCAV 1303 model has a slightly higher ratio than that of the model with elevons. Having elevons on the wings would result in a variation for the coefficients of pitching moment C_{MP} (Fig. 6(c)), particularly at $\alpha \approx 8°$, where the UCAV 1303 model tends to experience pitch break. The plot shows an increase in C_{MP} at this particular α compared with the baseline case. We suspect that the elevation in C_{MP} at low α is due to the increase of lift near the trailing edge of the wing (due to elevon), which would result in a nose-down pitch coefficient of moment.

Finally, the elevons generate a roll mode tendency that can be observed in the coefficients of rolling moment C_{MR} plot (Fig. 6(d)). The geometry variation due to the elevon on one of

https://doi.org/10.1017/aer.2021.15 Published online by Cambridge University Press

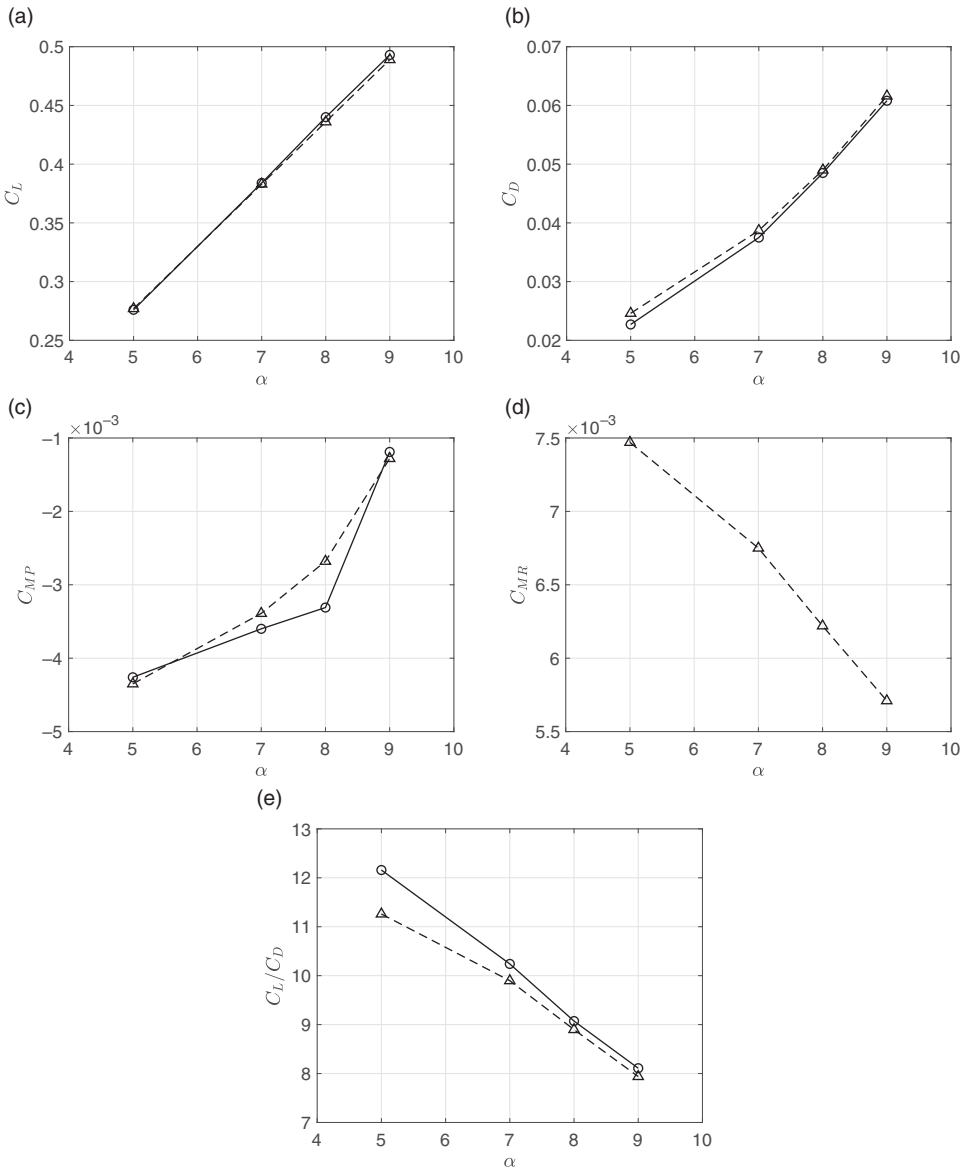

Figure 6. (a) C_L, (b) C_D, (c) C_{MP} and (d) C_{MR}, (e) L/D for the elevons as flow control against the baseline case. Solid lines with open circle represents the baseline case, and the dashed line with open triangles represents the elevon case.

the wings causes a change in the pressure difference between the top and lower part of the wing, resulting in a tendency to roll. The coefficients of rolling moment decrease with the angle-of-attack, which is probably due to the elevon's location (at the trailing edge). As α increases, the leading edge vortices that are generated by the UCAV 1303 become stronger and larger (Fig. 4). This would cause the flow around the trailing edge to be entrained into the recirculation region behind the large-scale leading-edge vortices, resulting in a reduced C_{MR}.

https://doi.org/10.1017/aer.2021.15 Published online by Cambridge University Press

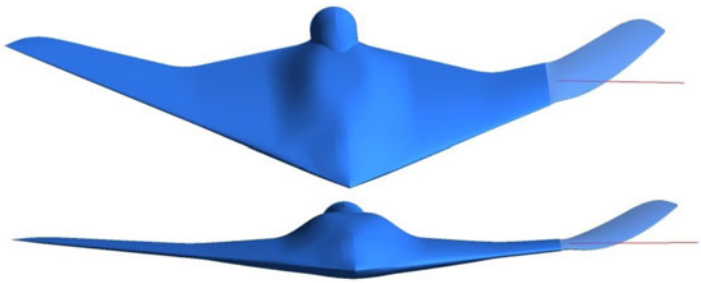

Figure 7. Illustration of UCAV 1303 with a 30° linear twist applied to one of the wings about the red-line axis.

4.2 Morphing wing case 1: linear twists

The first morphing case that we investigate is a linear twist. The linear twist aims to reduce the wing's local angle-of-attack while it generates a rolling moment and delays pitch break simultaneously. The morphed wing is designed to delay the onset of pitch break by lowering the wing's effective angle-of-attack, particularly over the area where the pitch break occurs. Thus it would allow the wing to maintain an attached leading-edge vortex. Here the linear twist is applied at the outer third of the wing ($\eta > 0.7$), which results in a gradual twist configuration along the axis of interest (Fig. 7). Here only one of the wings is twisted (port side). For this study, we conducted two linear twist cases: 10° and 30°. Note that the twist angles are referred to as the total twist at the wing tip; therefore, for a 30° linear twist angle, at an angle-of-attack of 5°, the wing tip would have an effective angle-of-attack of $5° - 30° = -25°$. Note that we did not conduct a morphing wing twist at 5° on one of the wings, which would have matched the elevon's angle. This is because one of the main aims of this investigation is to eliminate or delay pitch break; a low wing-twist angle such as 5° is not as effective as higher twist angles.

Figure 8 shows the aerodynamic characteristics of UCAV 1303 when it undergoes a linear twist at angles 10° (dashed lines with cross sign) and 30° (dashed lines with plus sign), the elevon case (dashed line with open triangles), and the baseline case (solid lines with open circles). Figure 8(a) illustrates the coefficient of lift C_L at various angles of attacks α; here the plot shows a vertical downward shift with increased linear twist angles. The reduced C_L is due to the change in the effective angle-of-attack due to twisting. The coefficient of drag C_D in Fig. 8(b) shows that, at a low angle-of-attack ($\alpha = 0° - 5°$), the twisted wing cases show a higher C_D than that of the baseline case. The higher C_D may be due to the increased wing twisting that causes the model to behave more like a bluff body. At a higher angle-of-attack ($\alpha = 7° - 15°$), however, the C_D is lower because the twisted wings effective angle-of-attack was closer to 0°, resulting in a more streamlined wing fuselage. Note that, even with the lower drag C_D, the maximum C_L/C_D of the twisted wings, at $\alpha = 5°$, is still lower than that of the baseline case (Fig. 8(e)). At a higher angle-of-attack ($\alpha > 7°$), the C_L/C_D ratio of the twisted wing cases show slight improvement compared with the baseline cases. The elevon case, on the other hand, has almost negligible influences on the C_D and C_L, as we have shown in the previous section.

The coefficients of pitching moment C_{MP} due to linear twist are illustrated in Fig. 8(c). From the plot, It is clear that linear twisting does not prevent the onset of pitch break. The UCAV 1303 still experiences pitch break at $\alpha \approx 8° - 9°$. However, it is clear that the difference in C_{MP} magnitude between the lower α ($\alpha < 8°$) and higher alpha ($\alpha > 8°$) for the twisted

https://doi.org/10.1017/aer.2021.15 Published online by Cambridge University Press

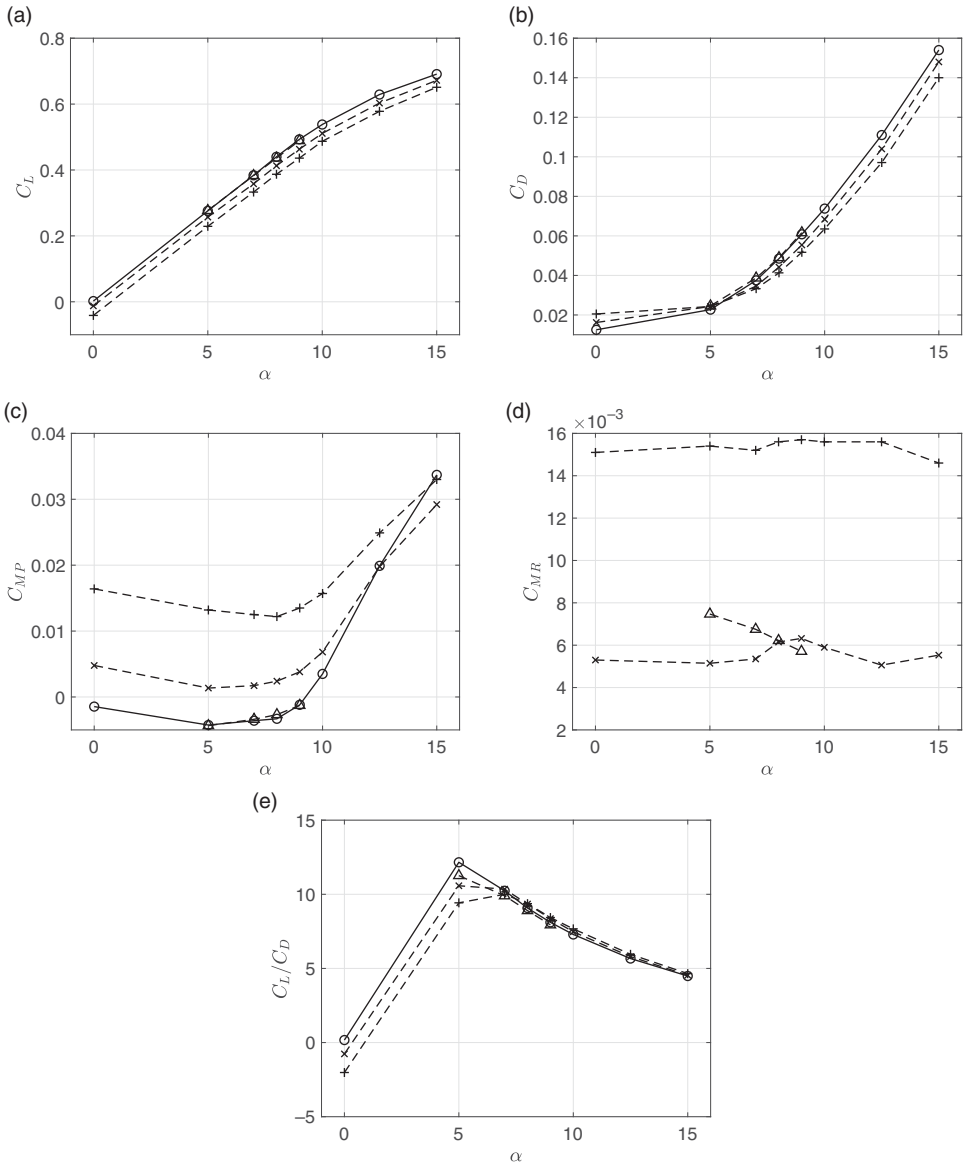

Figure 8. (a) C_L, (b) C_D, (c) C_{MP} and (d) C_{MR}, (e) L/D for various linear twists. Solid lines with open circle represents the baseline case, dashed lines with cross sign the 10° linear twist case, dashed lines with plus sign the 30° linear twist case and dashed line with open triangles the elevon case.

wing cases are smaller than that of the baseline cases;in other words, the C_{MP} profiles on the twisted wing cases at low α are shifted up when compared with the baseline case. Hence, twisting the UCAV 1303 wing influences C_{MP}, and reduces the difference in C_{MP} magnitude with respect to α. At very high angle-of-attack, $\alpha > 13$, the pitching moment coefficients of the twisted wing have a tendency to merge into the baseline case. It seems that this is due to the large-scale leading-edge vortical structures that are formed closer to the nose tip and leave the trailing edge closer to the UCAV-1303 centreline. Referring back to Fig. 4(e) and (f),

https://doi.org/10.1017/aer.2021.15 Published online by Cambridge University Press

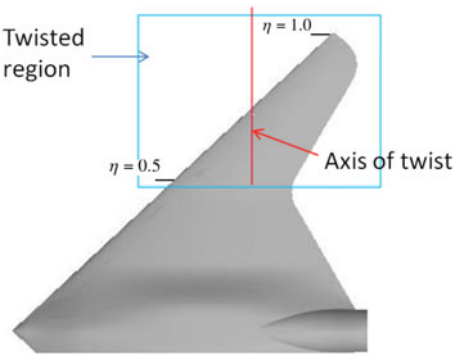

Figure 9. Location of linear wing twist for the ±5° washout and wash-in cases.

the majority of the large-scale leading-edge vortical flows at a high angle-of-attack ($\alpha > 12.5°$) leave the wing at trailing edge location of $\eta \approx 0.5$, near the rear concavity. Furthermore, note that the linear twisting happens at the outer third of the wing ($\eta > 0.7$). Therefore, the twisting has an only partial or small influence on the large-scale vortical structures, which in turn results in small change in C_{MP} at high α. Note that the C_{MP} vertical shifting of the twisted wing cases (Fig. 8(c)) is much more aggressive than in the case of the elevon, because the twist angle (10° and 30°) is higher than the elevon angle (5°). We did not conduct elevon simulation at a higher angle because of the small influence on the models coefficients of pitching moment. In these cases, there is only one wing that is twisted; hence, although the twisted wings may influence (or possibly reduce) the pitch break, the other wing side would still experience pitch break.

Figure 8(d) shows the coefficients of rolling moment C_{MR} for both the 10° and 30° twisted wings. Here we also include the elevon case as a comparison. Note that for the baseline case, there are no changes in C_{MR}, as it is zero. For both twisted wing cases, we can see that there is a variation of C_{MR}, albeit it is fairly steady at α. The variation in the coefficients of rolling moment is due to the twisting of one of the wings, which results in a rolling tendency for the UCAV 1303 model. Here we can see that the 30° twist case generates a much larger C_{MR} ($\approx 3\times$) than that of the 10°. The higher twist angle would translate into a higher pressure difference between the top and lower part of the wing, resulting in a higher roll tendency. The elevon 5° case seems to have higher coefficients of roll moment than that of the 10° twisted wing, particularly at a lower angle-of-attack ($\alpha < 8°$).

4.3 Morphing wing case 2: wash-in and washout

In the previous section, we have shown that the linear twist cases are not able to prevent or delay the onset of pitch break, although the magnitude is reduced. This condition is probably due to the pitch break forming very near to the wing tip; hence, it is not delayed significantly by the wing twist. To test this hypothesis, a less aggressive linear twists (5°) is applied at both wing ends over a larger area of the wing, starting from the concavity of the trailing edge at $\eta = 0.5$ (Fig. 9). As a comparison, the previous linear twist cases (where only one side of the wing twisted) occur at $\eta = 0.6$. The twisting of both wings would result in them behaving more like traditional washout and wash-in configurations. Washout can be defined as *"inbuilt wing twist resulting in an angle of incidence reducing towards tips"*[31], while wash-in is the opposite, where the angle of incidence is increasing towards the wing tip. Figure 10 illustrates

https://doi.org/10.1017/aer.2021.15 Published online by Cambridge University Press

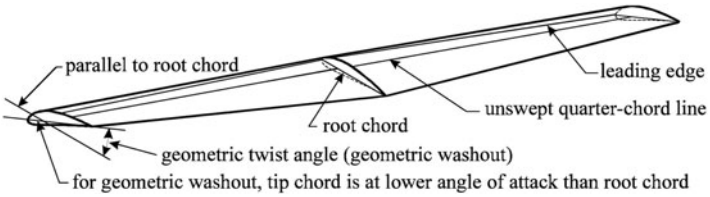

Figure 10. Illustration of washout (taken from Ref. (32)).

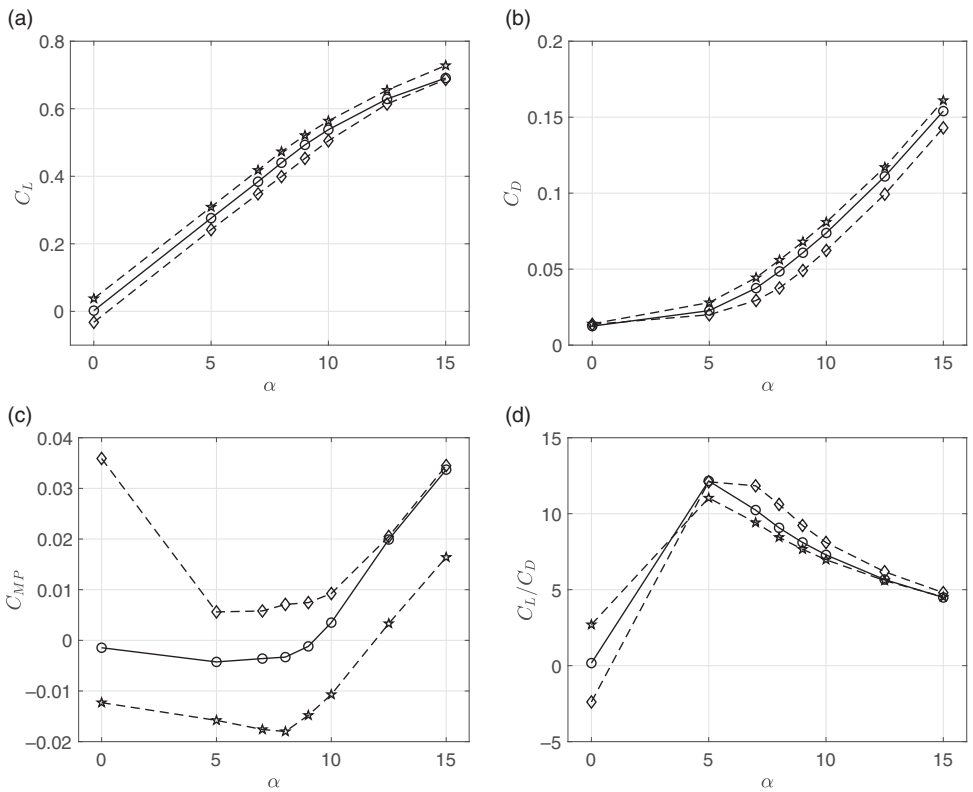

Figure 11. (a) C_L, (b) C_D, (c) C_{MP} and (d) C_{MR}, (e) L/D for wash-in and washout. Solid lines with open circle represent the baseline case, dashed lines with diamond markers the washout case and dashed lines with pentagram markers the wash-in case.

the definition of washout for further clarification[32]. Note that some of the initial results from this section have been reported by Brett et al. (2010)[33].

Figure 11 shows the aerodynamic coefficients for the baseline case (solid lines with open circles), washout case (dashed lines with diamond markers) and wash-in case (dashed lines with pentagram markers). The coefficient of lift and drag plots in Fig. 11(a) and (b) shows that the washout case has a lower coefficient than that of the baseline case, while the wash-in case has a higher coefficient than the baseline case. The lower coefficient of lift C_L of the washout case is similar to that of linear twist from one of the wings in the previous section. The reduced C_L is caused by the reduced effective surface area of the wings (due to the twisting). Hence,

https://doi.org/10.1017/aer.2021.15 Published online by Cambridge University Press

the higher the washout angle, the lower the lift coefficient will be (when it is compared with the baseline case). On the other hand, the wash-in configuration would allow the wing to have a greater surface area, resulting in an increased lift coefficient. With regard to the coefficient of drag, the washout case has a lower coefficient of drag C_D compared with the regular wings because of the twisted wing angle forces the wings effective angle-of-attack closer to 0°. This would result in a more streamlined UCAV-1303 at higher α, i.e. the C_D profile shifts to the right. For the wash-in case, however, the effective angle-of-attack of the wing would always be higher than that of its intended α. A higher effective angle-of-attack would result in a C_D increase higher than the base model, i.e. the coefficient of drag is shifted to the left. Interestingly, however, when we account for the C_L/C_D ratio (Fig. 11(d)), the washout case shows a better ratio than the wash-in case. The C_L/C_D ratio is higher than the baseline case, suggesting that the washout case has better aerodynamic performance than the wash-in case. The improved C_L from the wash-in case raises questions regarding how it would fare with the other flow control methods. A popular flow control technique that is often applied to UCAV 1303 is plasma actuators[15-18]. When compared with the plasma actuator technique, our C_L performs better, i.e. when it is compared with the baseline case, the C_L from our wash-in case is higher than the plasma actuator technique. However, the C_D result is not as good as the plasma actuator method. The C_D from wash-in is higher than the baseline case, while the plasma actuator method gives lower C_D.

The pitching moment coefficient figure (Fig. 11(c)) shows that the washout case shifts the C_{MP} values upwards when it is compared with the baseline case, particularly at $\alpha < 12.5°$. Beyond this angle, it seems that the washout has little effect on the pitching moment coefficient (similar to the one-wing linear twist in the previous section). The similar behaviour of the washout C_{MP} and baseline case C_{MP} at α beyond 12.5° is due to the location where the large-scale leading-edge vortices leave the wing trailing edge. Figure 4(e) and (f) have shown that, at $\alpha > 12.5°$, the large-scale leading-edge vortices leave the wing trailing edge at $\eta \approx 0.5$, near the concavity, while the twisting happens at the outer third of the wing ($\eta > 0.7$). Hence, the washout twist has a small influence on the large vortical structures on the trailing edge. The wash-in case, on the contrary, shows that it generates a reduced C_{MP} with α, relative to the baseline case. Both wash-in and washout cases show that they do not significantly modify the onset of pitch break (which is around $\alpha \approx 8° - 9°$). This may indicate that the twisting effect is too weak or the leading edge vortices detach further upstream before the twisting location. Although the wash-in and washout are unable to prevent pitch break or change the onset of pitch break, they may be useful for flight control purposes, for example, as a temporary shift in pitching moment that would lead to the increase or decrease of aircraft pitch angle.

Figure 12 shows the contours of the coefficient of pressure C_P and wall shear lines, for the (a) baseline case, (b) washout case and (c) wash-in case, at $\alpha = 10°$. This angle-of-attack is chosen because it is slightly after the onset of pitch break. The washout wall shear lines have a similar flow pattern to the baseline case. Here, the pressure at the leading edge of the washout case is low at $\eta \approx 0.5$ and after the concavity in the trailing edge where the twist begins. Furthermore, the pressure remains weaker over the outer wing $\eta \approx 1.0$, which would account to the loss in lift and an increase in pitching moment.

The wash-in case has a unique effect on the airflow; here the pressure is low at $\eta \approx 0.5$, but the pressure remains strong as the vortex travels down the wing until the point of vortex detachment at the outer wing $\eta \approx 1.0$. Such results come from the combination of upwards twist (increasing C_P) and bringing the wing upward towards the vortex slightly. Interestingly, both of these cases of geometry morphing do not appear to have a significant effect on the detachment location of the leading-edge vortex.

https://doi.org/10.1017/aer.2021.15 Published online by Cambridge University Press

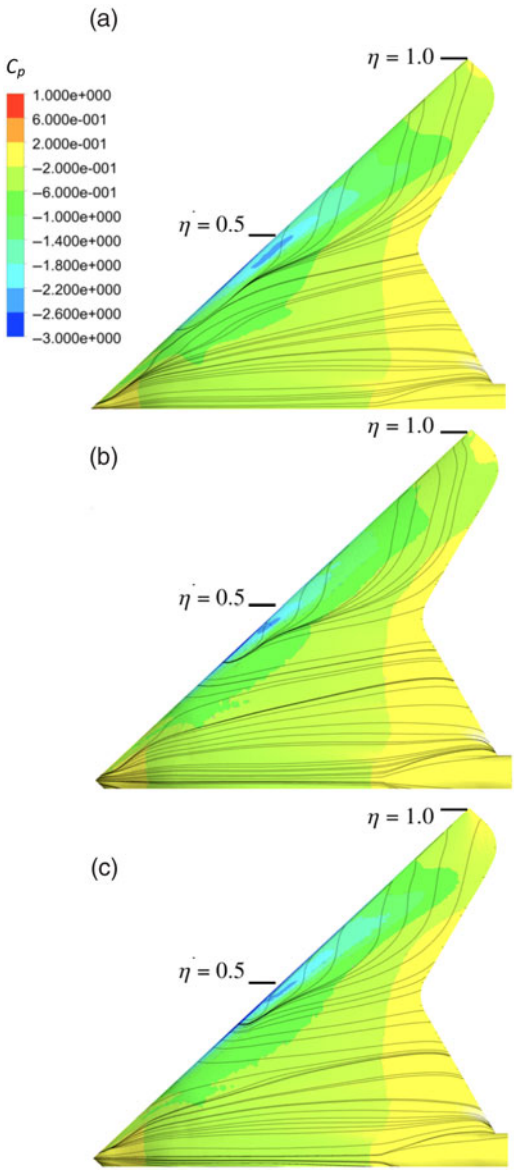

Figure 12. Contours of coefficient of pressure C_P and wall shear lines, for the (a) baseline case, (b) washout case and (c) wash-in case, at $\alpha = 10°$.

5.0 CONCLUSION

In this report, we have conducted several CFD simulations on UCAV 1303, which include baseline model and various wing geometric modifications. The baseline simulation results have good agreement with the experimental data in the literature, particularly for the C_D, C_L and C_{MP}. The baseline simulation results provided confidence to conduct further studies on wing profile geometric modifications. A geometric modification in the form of elevon and linear twist morphing (10° and 30°) was conducted on one of the UCAV 1303 wings. The

https://doi.org/10.1017/aer.2021.15 Published online by Cambridge University Press

aim of the linear twist is to produce rolling moment and to delay pitch break simultaneously. The coefficient of rolling moment C_{MR} from the linear twist is relatively small, independent of the angle-of-attack α, and has a magnitude comparable to the elevon results. The higher linear twist angle (30°) generates a larger C_{MP} magnitude, approximately three times larger than the 10° twist case. The large coefficient of pitching moment may prove to be useful for manoeuvring capabilities and can offer improvements in several other areas, i.e. stealth or reliability.

The wash-in and washout morphing geometry shows that it has a significant influence on the coefficient of lift, coefficient of drag and the pitching moment coefficient over a wide range of α. The washout case seems to be more promising because of its ability to generate an improvement of the C_L/C_D ratio over the entire angle-of-attack envelope. If we assume that the UCAV 1303 is properly trimmed to fly steadily at the desired α, a temporary morph such as wash-in and washout would produce a rapid desirable change in its flying characteristics. In short, the morphing wing has plenty of potential for future UCAV, such as UCAV 1303. Further investigation into a more aggressive or sophisticated morphing geometry is needed to extract the full potential of such capability. Note that for real morphing wing applications, a vast possibility of potential geometries exists. Since morphing occurs over a finite time duration, in addition to studying the geometries, the transient influence of the morphing wing is another aspect that can be studied.

REFERENCES

1. WOOLVIN, S. Conceptual design studies of the 1303 configuration, 24th AIAA Applied Aerodynamics Conference, American Institute of Aeronautics and Astronautics, 2006. DOI: 10.2514/6.2006-2991
2. WOOLVIN, S. UCAV configuration & performance trade-offs, 44th AIAA Aerospace Sciences Meeting and Exhibit, American Institute of Aeronautics and Astronautics, 2006. DOI: 10.2514/6.2006-1264
3. MCPARLIN, S., BRUCE, R., HEPWORTH, A. and RAE, A. Low speed wind tunnel tests on the 1303 UCAV concept, 24th AIAA Applied Aerodynamics Conference. American Institute of Aeronautics and Astronautics, 2006. DOI: 10.2514/6.2006-2985
4. BILLMAN, G.M. and OSBOURNE, B.A. High l/d extended range/payload fighter aircraft technology. AFRL-VA-WP-1999-3084, 1998.
5. ORDOUKHANIAN, E. and MADNI, A.M. Blended wing body architecting and design: Current status and future prospects. *Procedia Comput. Sci.*, 2014, **28**, pp 619–625. DOI: 10.1016/j.procs.2014.03.075
6. BILLMAN, G.M. and OSBOURNE, B.A. High l/d extended range/payload fighter aircraft technology. AFRL-VA-WP-1999-3084y, 1998.
7. BRUCE, R. High speed wind tunnel tests on the 1303 UCAV concept, 24th AIAA Applied Aerodynamics Conference, 2006.
8. ZHANG, F., KHALID, M. and BALL, N. A CFD based study of UCAV 1303 model, 23rd AIAA Applied Aerodynamics Conference, American Institute of Aeronautics and Astronautics, 2005. DOI: 10.2514/6.2005-4615
9. PETTERSON, K. CFD analysis of the low-speed aerodynamic characteristics of a UCAV, 44th AIAA Aerospace Sciences Meeting and Exhibit. American Institute of Aeronautics and Astronautics, 2006. DOI: 10.2514/6.2006-1259
10. CHANDRASEKHARA, M.S. and MCLAIN, B.K. Aerodynamic studies over a manoeuvring UCAV 1303 configuration, *Aeronaut. J.*, 2013, **117**, (1190), pp 445–465. DOI: 10.1017/s0001924000008095
11. CHANDRASEKHARA, M.S., SOSEBEE, P.D. and MEDFORD, C.M. Water tunnel force and moment studies of a manoeuvring UCAV 1303 and their control, 28th International Congress of the Aeronautical Sciences, American Institute of Aeronautics and Astronautics, 2012.
12. CHUNG, J. and GHEE, T. Numerical investigation of UCAV 1303 configuration with and without simple deployable vortex flaps, 24th AIAA Applied Aerodynamics Conference, American Institute of Aeronautics and Astronautics, 2006. DOI: 10.2514/6.2006-2989

https://doi.org/10.1017/aer.2021.15 Published online by Cambridge University Press

13. JEONG, B., LEE, D., SHIM, H., AHN, J., CHOI, H.L., PARK, S.O. and OH, S.Y. Yaw-control spoiler design using design of experiments based wind tunnel testing, *J. Aircraft*, 2015, **52**, (2), pp 713–718. DOI: 10.2514/1.c032747
14. LEE, J., LEE, S. and KIM, C. Actuations of synthetic jets on a UCAV planform at high angles of attack, 8th AIAA Flow Control Conference. American Institute of Aeronautics and Astronautics, 2016. DOI: 10.2514/6.2016-3171
15. PATEL, M.P., NG, T.T. and VASUVEDAN, S. Plasma actuators for hingeless aerodynamic control of an unmanned air vehicle, AIAA Paper 2006-3495, American Institute of Aeronautics and Astronautics, 2006.
16. PATEL, M.P., NG, T.T., VASUDEVAN, S., CORKE, T.C. and HE, C. Plasma actuators for hingeless aerodynamic control of an unmanned air vehicle, *J. Aircraft*, 2007, **44**, (4), pp 1264–1274. DOI: 10.2514/1.25368
17. LOPERA, J., NG, T., PATEL, M., VASUDEVAN, S. and CORKE, T. Aerodynamic control of 1303 UAV using windward surface plasma actuators on a separation ramp, 45th AIAA Aerospace Sciences Meeting and Exhibit, American Institute of Aeronautics and Astronautics, 2007. DOI: 10.2514/6.2007-636
18. NELSON, R., CORKE, T., HE, C., OTHMAN, H., MATSUNO, T., PATEL, M. and NG, T. Modification of the flow structure over a UAV wing for roll control, 45th AIAA Aerospace Sciences Meeting and Exhibit, American Institute of Aeronautics and Astronautics, 2007. DOI: 10.2514/6.2007-884
19. LENTINK, D., MÜLLER , U.K., STAMHUIS, E.J., DE K, R., VAN GEST, W., VELDHUIS, L.L.M., HENNINGSSON, P., HEDENSTRÖM , A, VIDELER, J.J. and VAN LEEUW, J.L. How swifts control their glide performance with morphing wings, *Nature*, 2007, **446**, (7139), pp 1082–1085. DOI: 10.1038/nature05733
20. WEISSHAAR, T.A. (ed.) *Morphing Aircraft Technology - New Shapes for Aircraft Design*, volume Overview 1. Neuilly-sur-Seine, France: Multifunctional Structures/Integration of Sensors and Antennas, 2006.
21. BOWMAN, J., SANDERS, B. and WEISSHAAR, T. Evaluating the impact of morphing technologies on aircraft performance, 43rd AIAA/ASME/ASCE/AHS/ASC Structures, Structural Dynamics, and Materials Conference, American Institute of Aeronautics and Astronautics, 2002. DOI: 10.2514/6.2002-1631
22. BOWMAN, J., SANDERS, B., CANNON, B., KUDVA, J., JOSHI, S. and WEISSHAAR, T. Development of next generation morphing aircraft structures, 48th AIAA/ASME/ASCE/AHS/ASC Structures, Structural Dynamics, and Materials Conference, American Institute of Aeronautics and Astronautics, 2007. DOI: 10.2514/6.2007-1730
23. WONG, M., MCKENZIE, G., OL, M., PETTERSON, K. and ZHANG, S. Joint TTCP CFD studies into the 1303 UCAV performance: first year results, 24th AIAA Applied Aerodynamics Conference. American Institute of Aeronautics and Astronautics, 2006. DOI: 10.2514/6.2006-2984
24. ARTHUR, M. and PETTERSON, K. A computational study of the low-speed flow over the 1303 UCAV configuration, 25th AIAA Applied Aerodynamics Conference, American Institute of Aeronautics and Astronautics, 2007. DOI: 10.2514/6.2007-4568
25. MONK, D. and CHADWICK, E.A. Comparison of turbulence models effectiveness for a delta wing at low Reynolds numbers, EUCAS Conference, 2017.
26. TOURNOIS, J., WORMSER, C., ALLIEZ, P. and DESBRUN, M. Interleaving Delaunay refinement and optimization for practical isotropic tetrahedron mesh generation, *ACM Trans. Graphics*, 2009, **28**, (3).
27. SI, H. Adaptive tetrahedral mesh generation by constrained Delaunay refinement, *Int. J. Numerical Methods Eng.*, 2008, **75**, (7), pp 856–880.
28. HUTCHINS, N. and MARUSIC, I. Large-scale influences in near-wall turbulence, *Philosophical Trans. R. Soc. A*, 2007, **365**, pp 647–664.
29. HUTCHINS, N. and MARUSIC, I. Evidence of very long meandering streamwise structures in the logarithmic region of turbulent boundary layers, *J. Fluid Mech.*, 2007, **579**, pp 1–28.
30. BRUCE, R.J. and MUNDELL, A.R.G. Low speed wind tunnel tests on the 1303 UCAV concept, Tech Rep QinetiQ/FST/TR025502/1.0, QinetiQ, 2003.
31. GUNSTON, B. *The Cambridge Aerospace Dictionary*, Cambridge University Press, 2004, Cambridge.
32. PHILLIPS, W.F. Lifting-line analysis for twisted wings and washout-optimized wings, *J. Aircraft*, 2004, 41, (1), pp 128–136.
33. BRETT, J., TANG, L., HUTCHINS, N. and OOI, A. Computational fluid dynamics analysis of the 1303 unmanned combat air vehicle, 17th Australasian Fluid Mechanics Conference, 2010.